JOURNAL OF THERMOPHYSICS AND HEAT TRANSFER
Vol. 24, No. 2, April–June 2010

Emissivity of Aluminum-Oxide Particle Clouds: Application to Pyrometry of Explosive Fireballs

Patrick Lynch,* Herman Krier,† and Nick Glumac‡
University of Illinois at Urbana–Champaign, Urbana, Illinois 61801

DOI: 10.2514/1.43853

Pyrometry measurements of clouds of high-temperature particles require an estimate of the spectral dependence of the particle emissivity. Common assumptions for this dependence range from $\varepsilon_\lambda \sim \lambda^{-2}$ to $\varepsilon_\lambda \sim$ constant. Depending upon the assumption used, there is uncertainty in the temperature of 100 s to a 1000 K in high-temperature clouds. Such errors are not apparent in goodness of fit of spectral data. A heterogeneous shock tube was used to measure the emissivity of aluminum oxide in an inert environment as a function of temperature (2000–3500 K), wavelength (0.55–0.95 μm), and particle diameter (50 nm–10 μm). In micro-sized alumina particles, the spectral dependence upon temperature transitions from decreasing with wavelength to increasing with wavelength with the dependence being roughly gray at about 3000 K. Because of local minima in the ε_λ vs λ curve, a power-law (λ^n) dependence is insufficient to describe the emissivity. However, if such a dependence is assumed, n transitions from −1.4 to 0.5 as temperature increases from 2500–3500 K. Nano-sized alumina particles exhibit an even stronger spectral dependence. At 2678 K, n is approximately −1.2 but reaches as high as 2.1 at 3052 K. Considering optical depth issues, there is merit in gray emissivity approximations for high-temperature (∼3000–3300 K) particles typical of aluminum particle combustion.

Nomenclature

C	=	power-law coefficient
c_n	=	third-order law coefficients, $n = 0, 1, 2, 3$
I_λ	=	spectral intensity, W m^{-2} μm^{-1}
n	=	power-law exponent
Q_a	=	spectral absorption efficiency
Q_s	=	spectral scattering efficiency
T	=	temperature, K
t_L	=	optical depth
ε_λ	=	spectral emissivity
λ	=	wavelength, μm
λ_0	=	reference wavelength, 1 μm

Subscripts

bb	=	Planck blackbody
cal	=	calibration source
exp	=	experimental
p	=	particle

I. Introduction

HIGH-TEMPERATURE particle thermometry is a common measurement (e.g., in evaluating the effects of an additive in a solid rocket motor engine or competing heterogeneous combustion mechanisms of burning metal clouds). Pyrometry is a nonintrusive optical measurement of condensed-phase temperature that can also be used to provide an indication of gas temperatures when atomic or molecular emission methods fail. All condensed-phase temperature measurements from spectral intensity require an assumption of the emissivity of particles or its spectral dependence. For example, in multicolor pyrometry, the continuum emission intensity in two or more wavelength regions (typically in the visible-to-near IR) are fit to a temperature [1]. However, an assumption needs to be made about the relative emissivity at the measured wavelengths of the particles. This effect is particularly important when the wavelengths of interest are separated by hundreds of nanometers, which is typically necessary to avoid local spectral biases and molecular interferences.

Common assumptions of the spectral dependence of alumina upon emissivity range from linear [2] to gray [3] to a λ^n dependence, where n is commonly −1 or −2 [4,5]. However, when fitting the intensities from different wavelengths to a temperature, as is done in Fig. 1 for 10 μm aluminum powder burning in air, the emissivity spectral dependence choice can lead to differences of hundreds, or even thousands, of degrees Kelvin in calculated temperature, which can lead to drastically different interpretation of combustion phenomena. The temperature is calculated by measuring the slope of the line formed by $\ell_n(I_\lambda \lambda^5/\varepsilon_\lambda)$ vs $1/\lambda$. For example, in Fig. 1, three choices are presented for the emissivity: $\varepsilon_\lambda \sim \lambda^{-2}$, $\varepsilon_\lambda \sim \lambda^{-1}$, and $\varepsilon_\lambda \sim 1$. Even taken over a considerable wavelength range (∼0.25 μm), these curves appear as lines, and no goodness-of-fit metric will allow the selection of the proper emissivity function. In Fig. 1, the R^2 value differs only by one part in 100,000, whereas the temperature measurement differs between 2792 and 3794 K.

Alumina was chosen for this study because of the prevalence of temperature measurements of reacting aluminum particles [6] in applications such as solid rocket motors. All aluminum is coated with an aluminum-oxide layer and condensed-phase alumina, which accumulates on a burning particle's surface and is the product of aluminum's reaction with O_2, CO_2, and H_2O. Recent results with similar conditions for larger particles (100–400 μm) show that the alumina cap on the aluminum surface dominates the emission from the particle. Furthermore, the oxide-smoke envelope around the flame zone accounts for another 5% of the intensity [7]. Because of this dominance of alumina emission during aluminum combustion, the properties of alumina are necessary to make temperature measurements. In previous measurements of alumina smoke in propellant flames, some variation in emissivity was observed that was likely due to trace metals, as well as sources other than alumina [8]. To isolate the effect of alumina, we use high-purity aluminum-oxide particles and conduct our experiments in argon. The inert particles also allow control of particle temperature by varying ambient conditions because no reaction is occurring, and thus the particle temperature quickly equilibrates to the ambient temperature.

Presented as Paper 640 at the 47th AIAA Aerospace Sciences Meeting, Orlando, FL, 4–8 Jan. 2009; received 16 Feb. 2009; revision received 3 Nov. 2009; accepted for publication 10 Nov. 2009.

*Ph.D. Student; ptlynch@illinois.edu. Member AIAA.
†Professor Emeritus; krier@illinois.edu. Fellow AIAA.
‡Professor, Mechanical Science and Engineering, 1206 West Green Street; glumac@illinois.edu. Member AIAA.

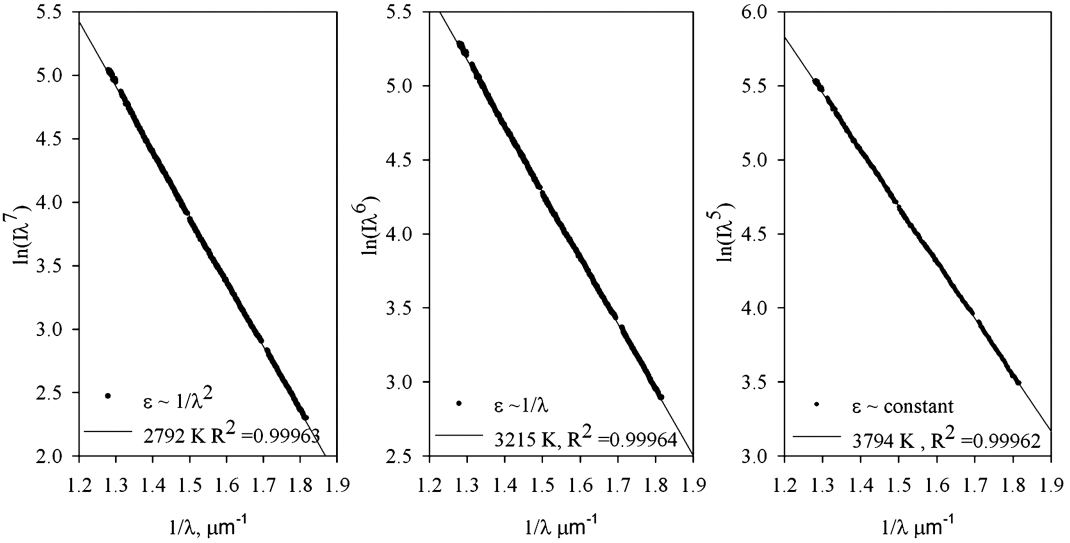

Fig. 1 The consequences of three different emissivity spectral dependence assumptions on temperature measurements for 10 μm Al powder burning in air.

Although an abundance of research exists as to the emissivity of slabs and other surfaces, including that of aluminum and alumina, and these are readily tabulated [9], the information on high-temperature particle emissivity necessary for temperature measurements is incomplete.

Good calculations [10] and data [8,11,12] are available for either limited wavelengths or longer wavelengths, typically 2–20 μm. However, measurements in the visible to *n*-IR (less than 1 μm) are needed because the high temperatures give high signals in the visible regions and these measurements are easier to make because of the availability of sensitive silicon or photomultiplier-based detectors in this spectral range. Additionally, data [13] are available for larger particles and lower temperatures, including where alumina is solid (less than 2300 K). Larger particles (1 mm, for instance) behave much closer to slabs or films than to particles. Smaller particles (smaller than class 10 μm) have full Mie scattering effects [5,14,15] that add complexity to their emissivity. Plass [16] has calculated the absorption dependence for particle sizes 100 nm–10 mm but with temperatures less than 2300 K. Additionally, the Plass data set, as discussed in [17], was most uncertain in the visible portion of the spectrum. A phase transition from solid to liquid results in an increase in overall emissivity, but the dependencies on temperature and wavelength at combustion temperatures (~2500–3500 K) are unclear.

II. Experimental Methods

The heterogeneous shock-tube facility at the University of Illinois generates a high-temperature, high-pressure controlled environment ideal for making measurements in combustion conditions. The driven section (the test section) is 8 m long and 8.9 cm internal diameter. Other relevant dimensions and descriptions of this facility can be found in previous publications [2,18,19]. Through the pressure ratio of the driver and driven sections, a strength-selectable shock can produce a controlled combustion environment for approximately 2 ms in this shock tube. Various compositions of test gases can be used. Temperatures exceeding 4000 K and pressures up to 30 atm are achievable.

Figure 2 shows the experimental setup and diagnostics used in this experiment. Approximately 1 mg of particles were injected into the shock tube from a port 0.68 m from the endwall approximately 1 s before the rupture of the double-diaphragm section. Nano particles may be suspended for minutes, whereas larger particles may very quickly descend to the bottom of the shock tube within a second or two. The cloud of particles was accelerated toward the endwall in the gas behind the incident shock wave. The gas behind the reflected shock stagnated the particles in front of the diagnostic equipment and heated the particles to a controlled temperature where they emitted.

A cloud of suspended particles is needed in order to properly account for particle motion during the event and ensure that the diagnostics are properly focused. The injector used, which is diagrammed in Fig. 3, is similar to that of Parker et al. [20]. Upon injection, a piston drives test gas though an insert loaded with powder into the shock tube. Brown [21] took high-speed images of the powder injection and redesigned the injector insert in order to maximize the suspension time of the cloud and the uniformity of the cloud throughout the cross section of the shock tube. A custom eight-hole (500 μm hole diameter) brass tip with a 8–32 insert set screw with a 500 μm hole drilled through it was used. The brass injector tip can hold 1–3 mg of powder. The insert set screw threads into the eight-hole brass tip but leaves a gap so that as the test gas is pushed through the insert set screw hole: the powder is entrained and passes through the eight-hole tip. The tip is encased in the larger insert body. At the exit of the tip, the powder passes through two fine meshes with 60 μm spacing to further disperse the cloud and break up agglomerates.

Two different size distributions of alumina were studied. Both were purchased from Alfa Aesar and have purities greater than 99.5%. These powders were not treated before being loaded into our injector. The first size distribution, micro alumina, had particles in the 0.9–2.2 μm range. The second powder, nano alumina, had a size distribution between 40–50 nm and specific surface area between 32–40 m^2/g. Figure 4 shows a scanning electron micrograph of the micro-alumina powder. These alumina particles were not uniformly spherical. Specifically, in the micro-alumina sample, there were some high-aspect-ratio particles and fibrous particles. The size distribution of the micro-alumina distribution is shown in Fig. 5. The number average was 1.56 μm, but the presence of a few larger

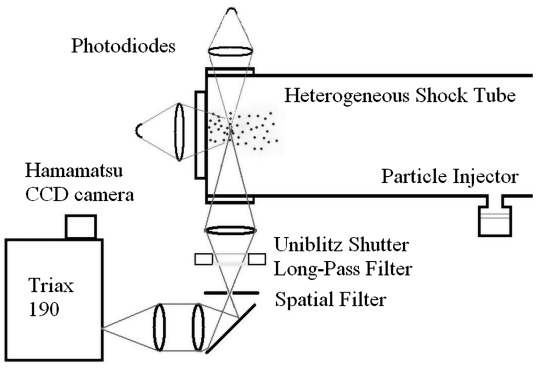

Fig. 2 Schematic of heterogeneous shock tube and diagnostics.

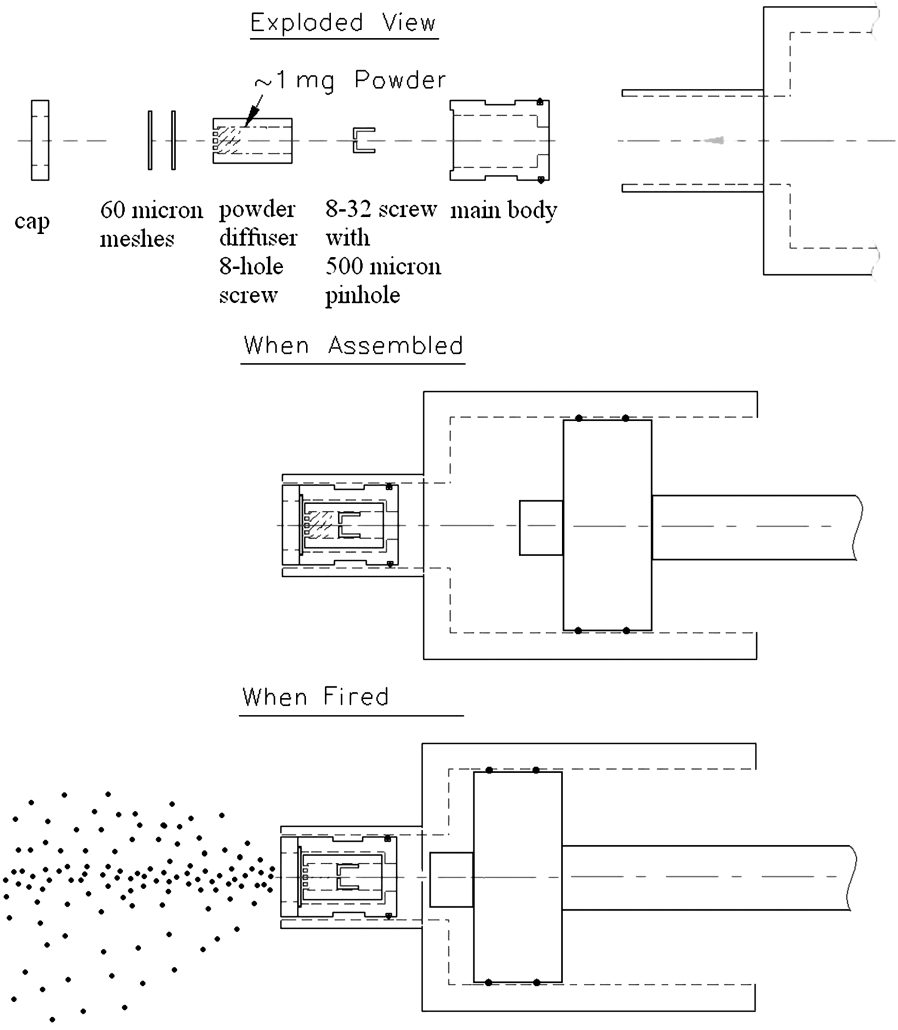

Fig. 3 Schematic of injection system.

particles skewed the surface area average to 2.89 μm. We were unable to measure a size distribution of the nano alumina in-house because nano-alumina particles were unsuitable for scanning electron micrograph (SEM). From previous studies with nano-aluminum powders [2,22], the nano-alumina powders should be more spherical, moderately agglomerated, and with a comparatively broad-size distribution.

Figure 4 also shows the tendency of alumina to agglomerate [23]. The larger agglomerates should have broken up during injection into the tube. Further, there is evidence that small particles become less agglomerated after the passing of the incident and reflected shocks [24,25]. In those studies, the breakup of agglomerates behind the incident shock was sufficient to counteract any sintering that may have happened in the higher-temperature gas. Finally, large agglomerates are accelerated less gradually in the stagnant gas behind the reflected shock. Our diagnostics were focused at a location calculated by our trajectory modeling of individual particles. Larger agglomerates are stopped either closer to the endwall than our diagnostics or

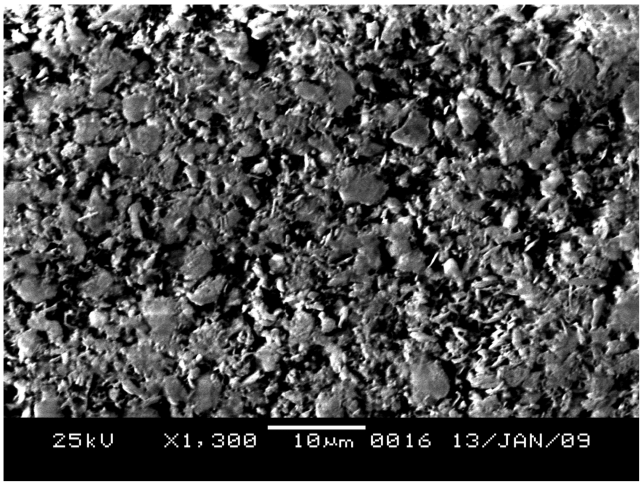

Fig. 4 SEM of micro alumina.

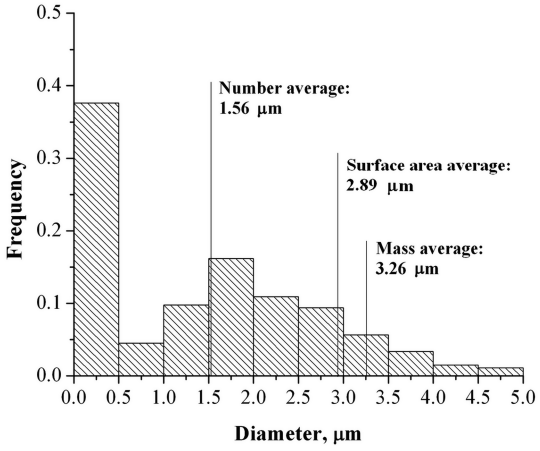

Fig. 5 Size distribution of micro alumina.

deposit on the endwall. In either situation, they would not have contributed significantly because of our spatial filtering.

A $f/8$ lens system collected the light from the emitting particles and passed it through a Triax 190 mm spectrometer with a 300 g/mm grating before being collected by a Hamamatsu back-thinned charge-coupled device (CCD) array. The optical train contained a 0.515 μm long-pass filter to eliminate order overlap, a Uniblitz shutter to control the exposure time, and a pinhole spatial filter to reject light away from the centerline of the shock tube. The shutter timer was changed under each temperature condition such that the intensity on each pixel of the CCD array was at least 10,000 counts (typically $\sim$30, 000) without saturating. The shutter was always closed by the end of the shock-tube test time. When necessary, neutral density filters were used to attenuate the signal when time resolution could not.

The spectral region of interest was between 0.55 and 0.95 μm. This region avoids molecular interferences of AlO at wavelengths lower than 0.54 μm while extending into the near IR. If molecular interferences are avoided, this region is suitable for making temperature measurements using pyrometry. To preserve dynamic range across the entire region, a Roscolux Apricot R68963 color filter was used to attenuate the signal at the blue end of the spectrum.

Intensity calibrations were taken with every change in condition. Intensity calibrations were carefully matched to exact experimental conditions. The primary intensity source was a 1273 K National Institute of Standards and Technology (NIST) traceable blackbody generator. This source provided ample signal for wavelengths larger than 0.7 μm. However, the intensity of the blackbody source was insufficient below 0.7 μm. To extend the range of this calibration, an Oriel tungsten lamp with nominal color temperature of 3200 K was used. The lamp was calibrated to a blackbody temperature using the spectral region between 0.7–0.95 μm using the NIST blackbody generator, and then this signal was used to generate an intensity calibration for wavelengths lower than 0.7 μm, where the signal level was ample, as shown in Fig. 6.

These particles were tested in 100% Ar, approximately 10 atm reflected shock pressure, and reflected shock temperatures starting at 2400 K and increasing up to 3500 K. This procedure was repeated for micro-alumina as well as nano-alumina samples, twice for each condition.

The emissivity of the particle at a given temperature was calculated using

$$\varepsilon_\lambda(T) \sim \frac{I_{\lambda,\mathrm{exp}}}{I_{\lambda,\mathrm{bb}}(T_p)} \frac{I_{\lambda,\mathrm{bb}}(T_{\mathrm{cal}})}{I_{\lambda,\mathrm{cal}}} \tag{1}$$

The emissivity calculation shows the proportionality of emissivity along wavelengths at a given temperature. The proportionality constant could not be calculated with this experiment because the absolute intensity (both of the experiment and the calibration) was not measured.

While the wavelength dependence on emissivity was measured, the absolute emissivity levels were estimated from an optically thin, full Mie scattering model [14,15] that accounts for the temperature dependence upon the optical constants [7,12], as well as the size distribution [26], albeit with spherical particles. Poleatev and Florko [12] had experimental data for the absorption index of the complex index of refraction at temperatures up to 3150 K. We extrapolated their values to higher temperatures (up to 3500 K) by using Shigapov's fit [27] for the scale and assumed the same spectral profile as Poleatev and Florko's 3150 K data [12].

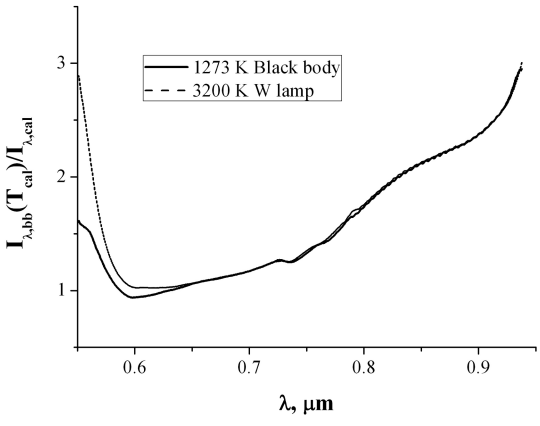

Fig. 6 A typical intensity calibration.

In this processing, ε_λ was taken as equal to Q_a [28,29], which we based on comparison to a least-squares fit over 0.55–0.9 μm. These absolute emissivity levels increase toward unity near 3500 K, which is an expected trend. We also attempted to calculate emissivity based on $\varepsilon_\lambda = 2.31(Q_a/Q_s)^{0.5}$ [30,31] because the scattering coefficient was so much larger than the absorption coefficient, however, the fits were even poorer because the assumption of a semi-infinite medium was invalid.

The amount of powder injected into the shock tube was about 1 mg, and previous results have shown that only a fraction of this powder is distributed over at least 10 cm in the test section after the reflected shock (the rest, initially wall bound, remained outside of the test section during the reflected shock period). If particles were distributed uniformly throughout this volume, there would have been about 75 particle diameters of spacing between particles. For the micro alumina, in the collection volume of the $f/8$ optics, there would have been approximately 10,000 particles, whereas there may have been as many as a billion nano-alumina particles. Any agglomeration even after the breakup behind the incident shock, may have significantly reduced these numbers. These numbers suggest the cloud of nano alumina was optically thicker than the cloud of micro-alumina particles, perhaps significantly.

We have, however, tested the extinction through a similar density of particles (approximately 1 billion in the same collection volume). We measured less than 5% extinction of light through that cloud, which suggests that clouds of particles in these configurations are optically thin. The assumption of uniform distribution of particles in the cloud is somewhat naive, as many particles are concentrated near the cloud front and are lost to the endwall.

Low optical depth is important to ensure that the intensity measurements are almost solely from emission of the particles, not from scattering or with a significant absorbed quantity, which would confound the wavelength dependence of emissivity. As optical depth increases, intensity measurements tend to approach gray dependencies as multiple scattering and absorption make a region increasingly resemble an isothermal cavity [5].

With such a high spacing of the particles, the heat capacity of the environment was about 150 times that of the particles, meaning that the particles heat up or the emission effect on the gas was well within the temperature uncertainty (25 K) from the reflected shock calculation. This effect was even smaller because the particles moved throughout the gas as they were heated. For this reason, the ambient temperature was the reflected shock temperature and was assumed to be unaffected by the low mass fraction of particles present.

The temperature of the particles, T_p, was set slightly less than that of the gas behind the reflected shock by a few degrees. A balance was calculated between the radiative loss of the particles (total emissivity was initially assumed at 0.3) and heat added to the particles from convection and conduction. The particles' velocity and temperature history was calculated by our trajectory modeling program [2], and the conditions behind the incident and reflected shock were calculated using Gaseq [32] from the measured shock velocity. The maximum temperature difference between the particles and ambient conditions was only 30 K, and the difference was more dependent upon ambient conditions than it was on the assumed emissivity.

The particle heat-up-time characteristic of the micro-alumina powder was 50 μs in raising the particle temperature from the incident shock ambient temperature to the reflected shock ambient temperature. This time was at most 4% of the integration time on the CCD array; however, because the intensity is proportional to T^4, it accounted for less than 2% of the integrated intensity and was within the shot noise. The heat-up-time characteristic of the nano powder was much smaller.

III. Results and Discussion

Figure 7 shows the spectral dependence of emissivity of the intensity calibrated emission from 2 μm Al_2O_3 in 100% Ar at about 3000 K. The emissivity is normalized to the value at 0.95 μm. Two conditions are shown. The first is 2985 K and the second is 3033 K. The broadband signals at these temperatures, when normalized, overlap to a great extent, showing very high repeatability. This repeatability was typical of the other conditions. At about 3000 K, the emissivity is roughly constant (i.e., gray) across wavelengths, but does increase at the shorter wavelengths.

Common molecular interferences of sodium and potassium are present for this and other conditions. These bands are ignored in the further analysis. There are, however, large regions in the spectra without interferences that are appropriate for taking pyrometry measurements. Once the atomic and molecular interference bands are removed from the emissivity calculation of Eq. (1), the resulting emissivity is subjected to 20-pixel (7 nm) smoothing. This smoothing does not affect the shape of the emissivity across the spectra, but it does reduce an experimental artifact of etaloning from the CCD array, which was prevalent at wavelengths larger than 0.7 μm. The effect was minimal, however, as the counts at each pixel differed by less than 2% of the value generated by the 20-pixel smoothing.

A. Micro Alumina

Figure 8 shows the emissivity of micro-alumina particles with respect to wavelength for temperatures between 2500 and 3500 K. The emissivity decreases with wavelength for temperatures below 2720 K, which is an expected and commonly assumed result. Near 3000 K, however, there is a slight decrease until about 0.77 μm, after which there is a slight increase. Overall, however, the emissivity is quite level. At higher temperatures, there is again the decrease to a local minimum. However, the local minimum occurs at lower wavelengths, about 0.65 μm for both 3360 and 3500 K. At these temperatures, however, the increase of emissivity with wavelength at higher wavelengths is not negligible.

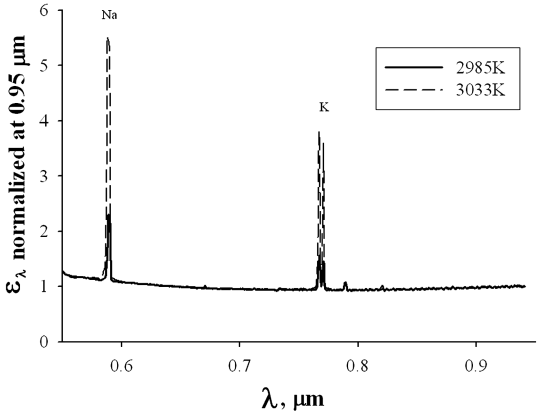

Fig. 7 Spectral dependence of emissivity for micro alumina near 3000 K.

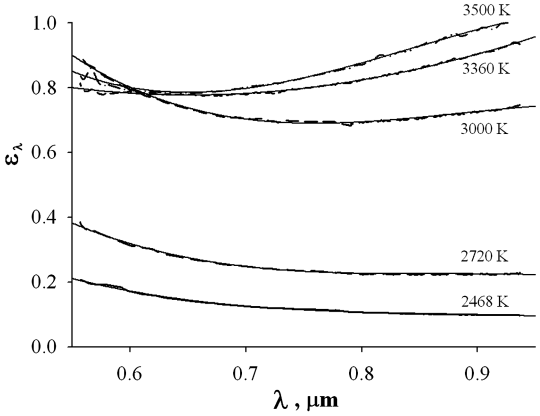

Fig. 8 Temperature dependence of emissivity (dashed lines) for micro alumina as well as a third-order polynomial fit to the data (solid lines).

Table 1 Emissivity wavelength dependence for micro alumina with temperature.

Temperature, K	c_0	c_1	c_2	c_3	R^2
2468	1.95	−6.26	7.12	−2.73	0.99
2720	3.48	−11.3	13.0	−5.02	0.99
3000	6.07	−18.9	21.9	−8.28	0.99
3360	1.89	−3.72	3.50	−0.66	0.98
3500	5.75	−19.3	24.2	−9.60	0.99

Table 2 Emissivity wavelength dependence for micro alumina with temperature.

Temperature, K	C	n	R^2
2468	0.082	−1.37	0.94
2720	0.194	−0.87	0.84
3000	0.677	−0.26	0.41
3360	0.911	0.34	0.76
3500	0.996	0.49	0.77

The emissivity of the micro alumina with temperature has been fit to both a third-order function of wavelength and a simple power law. A third-order equation was necessary to maintain the curvature of the emissivity throughout the wavelength region of interest for all temperatures. The emissivity is given by

$$\varepsilon_\lambda(T) \sim c_0 + c_1\left(\frac{\lambda}{\lambda_0}\right) + c_2\left(\frac{\lambda}{\lambda_0}\right)^2 + c_3\left(\frac{\lambda}{\lambda_0}\right)^3 \tag{2}$$

where λ is the wavelength in micrometers, $\lambda_0 = 1$ μm, and c_n are coefficients presented in Table 1. The third-order fitting was sufficient to maintain a fit of $R^2 > 0.98$. This fit is plotted along with the experimental data in Fig. 8.

We make a strong caution when using the third-order fit for emissivity to not extrapolate the wavelength dependence very far outside of the region of 0.55 to 0.95 μm because the polynomial fit necessarily has local extrema outside the region of interest. Within the region of interest, however, local minima were experimentally observed.

Additionally, the experimental emissivity measurement was also fit to a power of wavelength, using

$$\varepsilon_\lambda(T) \sim C\left(\frac{\lambda}{\lambda_0}\right)^{n(T)} \tag{3}$$

with coefficients given in Table 2. This fit is plotted in Fig. 9. The reason this fit was employed was because it is very easy to measure

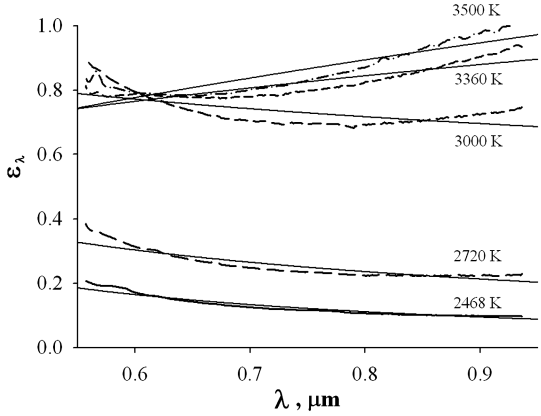

Fig. 9 Temperature dependence of emissivity (dashed lines) for micro alumina along with a power-law fit to the data in solid lines.

temperature as described in the introduction by the slope of $\ell_n(I\lambda^{5-n})$ plotted against $1/\lambda$. Additionally, a simple power-law fit gives the essential information on the strength and slope of the wavelength dependence. Depending upon the wavelength regions used in a pyrometric measurement, for example, this may be sufficient detail to make an improved temperature measurement.

With the possible exception of the lowest-temperature data at 2468 K, the dependence of emissivity on wavelength is more complex and is not well described by a simple λ^n law. The fits, although they show the broad trend, do not match the detail very well, and for the high-temperature data, miss the local minima completely. Indeed, the R^2 measure of goodness-of-fit ranges from as low as 0.4 to as high as 0.94, as shown in Table 2. Still, reporting the n value has the added benefit of providing an indication as to the quality of the assumptions used in making temperature measurements. Emissivity dependences varying like λ^{-2} or λ^{-1} are seemingly appropriate for low-temperature measurements, where the temperature is right beyond the melting temperature of alumina. However, at temperatures near 3000 K, a graybody assumption is seemingly appropriate, whereas up to 3500 K, a $\lambda^{1/2}$ or λ dependence is seemingly appropriate.

The complex emissivity temperature dependence is caused by the strong temperature dependence in the complex index of refraction of alumina [8,33]. Poletaev and Florko [12] saw a four-orders-of-magnitude difference between the imaginary (absorptive) component of the refractive index between 2300 and 3000 K. Further, although limited points were used in the visible spectrum, the trend of absorptive index shifted from decreasing with wavelength to increasing with wavelength in the range of 2900–3000 K between 0.5 and 1 μm.

B. Nano Alumina

The emissivity of nano alumina was also tested to compare size effects. The micro-alumina powder is larger but on the order of the wavelength ($\sim$1 μm). The nano-alumina powder ($\sim$50 nm), however, is less than one-tenth the wavelength of light, therefore the scattering regime should be different [14]. These results are shown in Fig. 10. Both the third-order fit for emissivity [Eq. (2)] and the power-law fit for emissivity [Eq. (3)] were calculated, and the proper coefficients are displayed in Tables 3 and 4, respectively. However, only the power-law fit is shown in Fig. 10. The fit for the third-order polynomial has a goodness-of-fit R^2 at 0.99 and again very closely resembles the experimental data.

At lower temperatures, the emissivity decreases with wavelength, whereas at higher temperatures, it increases with wavelength. The dependencies and transition, however, appear to be sharper than for micro alumina. The power-law dependence increases from $n = -1.2$ at 2678 K to $n = 2.1$ at 3052 K. In comparison, micro alumina at similar temperatures had $n = -0.9$ and -0.3, respectively.

Additionally, the signals from the nano alumina were much less intense than for the micro-alumina samples at the same temperature and the emissivity calculated using the absolute emissivity model

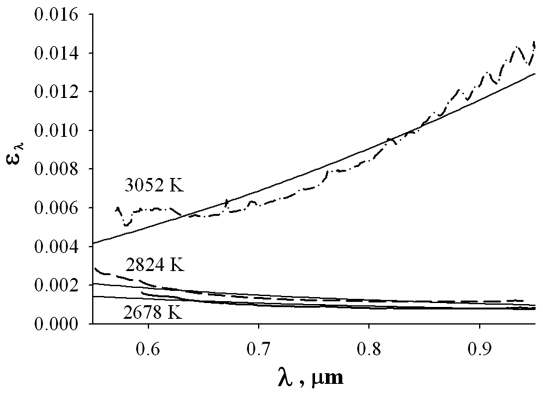

Fig. 10 Temperature dependence of emissivity (dashed lines) for nano alumina along with a power-law fit to the data in solid lines.

Table 3 Emissivity wavelength dependence for nano alumina with temperature.

Temperature, K	c_0	c_1	c_2	c_3	R^2
2678	0.0235	−0.0771	0.0871	−0.0327	0.99
2824	0.0422	−0.1472	0.1758	−0.0698	0.99
3052	0.0813	−0.2866	0.3359	−0.114	0.99

Table 4 Emissivity wavelength dependence for nano alumina with temperature.

Temperature, K	C	n	R^2
2678	0.0007	−1.19	0.79
2824	0.0009	−1.41	0.80
3052	0.0144	2.07	0.91

resided at a much lower overall level than for micro alumina. However, this prediction came from a region of the model, highest temperature and smallest particles, that contained the largest amount of extrapolated data, and therefore, although the relative emissivity dependence was fairly precise, the absolute emissivity had significant uncertainty. The absolute emissivity trends match those seen by Harrison and Brewster [33].

Finally, the optical depth of the nano-alumina clouds was greater than that of the micro-alumina clouds. Although similar configurations we have measured suggest that the nano-alumina cloud that we have measured was still optically thin, any scattering component would describe the strong wavelength dependence seen in higher temperatures. As particle size is approximately one-tenth the wavelength of light, Rayleigh scattering ($\sim\lambda^{-4}$) would more strongly scatter the shorter wavelength light and allow the longer wavelength light to reach the detector [15]. Additionally, as particle size decreases, particle morphology effects should become more important, including crystallinity. This could also explain differences seen between micro and nano alumina [34,35].

C. Application to Particle Temperature Measurements

Based on the experimental measurements of emissivity, we simulated the error associated with using the gray particle assumption. To do this, we assumed a 1-D homogeneous medium (a slab) of a certain optical depth and temperature. This medium emitted and interacted according to its measured emissivity. The expected result was a transfer function determined by measuring the spectral intensity beyond the interacting medium [5]:

$$I_\lambda \sim I_{\lambda,\mathrm{bb}}(T)(1 - \exp(-t_L)) \tag{4}$$

where t_L is the optical depth of the slab of homogeneous emitting particles, which is proportional to ε_λ. The limits for optical depth reduce to

$$\lim_{t_L \to 0} I_\lambda \sim I_{\lambda,\mathrm{bb}}(T) t_L \tag{5}$$

$$\lim_{t_L \to \infty} I_\lambda \sim I_{\lambda,\mathrm{bb}}(T) \tag{6}$$

This spectral intensity I_λ is then fit to a blackbody intensity at a specified temperature. The results of this simulation for micro-sized particles are shown in Fig. 11. The error in temperature calculated when assuming gray emissivity decreases with optical depth, as well as remaining low in the region of 3000–3300 K. Above 3300 K in optically thin conditions, the temperature is underpredicted by as high as 10%, whereas the temperature may be overpredicted by as much as 20% at 2500 K.

This result is fortuitous for two reasons: 3000–3300 K is a typical peak combustion temperature of particles in this size range measured both with pyrometric measurements [6] and measurements of the

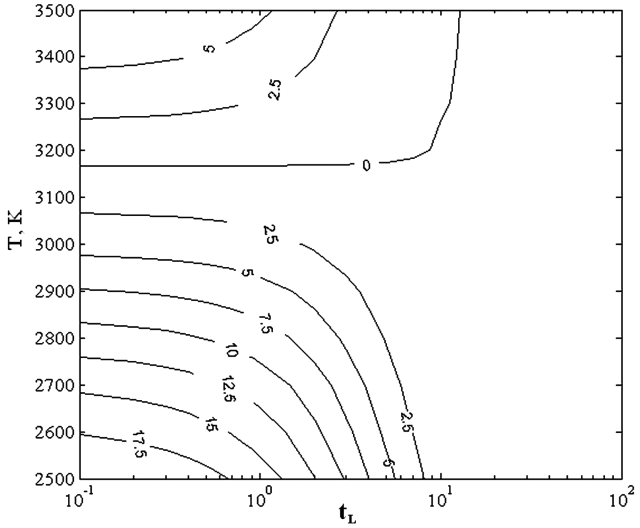

Fig. 11 Percent error in measured temperature associated with using gray emissivity assumption as a function of optical depth and particle temperature for micro alumina.

temperature of a gas-phase combustion intermediate (AlO) thought to be very close to that of the particle [36]. Other results for larger particles ($\sim$100 μm) showed peak temperatures in this range as well [3,37]. Furthermore, many applications of pyrometric particle temperature measurements, such as aluminum combustion in a propellant or a fireball, are made in conditions that are often optically thick.

Some of the limitations of this analysis are optical depth, presence of other emitters besides alumina, and size distribution. Optical depth is a significant limitation in measurements, and careful consideration of optical depth must be taken in temperature measurement applications. If measurements are made in optically thick particle clouds of inhomogeneous temperature, such as a propellant or a fireball, then the measured temperature will only be representative of the edge of the cloud and not of the core.

Although the emissivity is very high in this high-temperature region, a strong scattering component may change these results slightly. Additionally, although reacting aluminum particles are dominated by alumina emission, the presence of aluminum having a different emissivity spectral dependence will slightly alter the mean emissivity of a collection of particles. Finally, as has been described, the particle diameter has an effect on the emissivity dependence; therefore, the size distribution should be understood when making temperature measurements. For example, although the difference in measured temperature for micro- and nano-alumina particles would be less than 50 K at temperatures of about 2500 K, it may be as much as 1000 K at about 3000 K. The effects of agglomeration and the alumina-smoke cloud in particles where aluminum is burning suggest that the particles should be assumed larger rather than smaller should there be ambiguity in the size distribution.

As particle size increases, the gray assumption appears to give reasonable temperatures [3,36] and effects that cause deviations from gray-particle behavior appear negligible. Particularly, in the work by Dreizin [3], while using the gray-particle assumption, the temperature steadied at the melting temperature of the aluminum oxide after the high-temperature region, which is reasonable. In our work with 10 μm particles in the shock tube [6], also assuming gray particles, after the peak was reached during the reaction, the particle temperature decayed to the expected elevated ambient temperature within the test time. The ambient temperature and the latter particle temperature showed good agreement.

IV. Conclusions

An experimental study of the emissivity of micro- and nano-alumina particles was conducted in a shock tube for temperatures between 2500 and 3500 K in the wavelength region between 0.55 and 0.95 μm:

1) In micro-sized alumina particles, the spectral dependence with increasing temperature transitions from decreasing with wavelength to increasing with wavelength, with the dependence being roughly gray at about 3000 K.

2) Although a power-law λ^n dependence for emissivity is insufficient to describe the emissivity in this region, n transitions roughly from -1.4 to 0.5 as temperature increases from 2500 to 3500 K.

3) In nano-sized alumina particles, the spectral dependence is stronger than for the micro-sized particles, and although n is approximately -1.2 at 2678 K, it reaches as high as 2.1 at 3052 K.

4) A gray-particle emissivity assumption has merit for micro- and larger-size particles at combustion temperatures (3000–3300 K), especially considering optical depth effects in measurements.

Acknowledgments

This research was sponsored by the Defense Threat Reduction Agency under contracts HDTRA1-07-1-0011 and DAAE30-1-9-0080 (program managers William Wilson and Suhithi Peiris). The scanning electron micrographs were taken in the Frederick Seitz Materials Research Laboratory Central Facilities at the University of Illinois, which are partially supported by the U.S. Department of Energy under grant DEFG02-91-ER45439. We thank Quinn Brewster for helpful discussions and recommendations on this work. Thanks also go to Bryan Mooney, David Mesri, and Mark Figge for technical assistance.

References

[1] Panagiotou, T., Levendis, Y., and Delichatsios, M., "Measurements of Particle Flame Temperatures Using Three-Color Optical Pyrometry," *Combustion and Flame*, Vol. 104, No. 3, 1996, pp. 272–287. doi:10.1016/0010-2180(95)00119-0

[2] Bazyn, T., "Spectroscopic Measurements of the Combustion of Aluminum and Aluminum-Based Energetic Material Particles Using a Heterogeneous Shock Tube," Ph.D. Dissertation, Dept. of Mechanical and Industrial Engineering, Univ. of Illinois at Urbana–Champaign, Urbana, IL, 2006.

[3] Dreizin, E. L., "Experimental Study of Stages of Aluminum Particle Combustion in Air," *Combustion and Flame*, Vol. 105, No. 4, pp. 541–556. doi:10.1016/0010-2180(95)00224-3

[4] Goroshin, S., Mamen, J., Higgins, A., Bazyn, T., Glumac, N., and Krier, H., "Emission Spectroscopy of Flame Fronts in Aluminum Suspensions," *Proceedings of the Combustion Institute*, Vol. 31, No. 2, 2007, pp. 2011–2019. doi:10.1016/j.proci.2006.07.175

[5] Brewster, M. Q., *Thermal Radiative Transfer and Properties*, Wiley, New York, 1992.

[6] Glumac, N., Krier, H., Bazyn, T., and Eyer, R., "Temperature Measurements of Aluminum Particles Burning in Carbon Dioxide," *Combustion Science and Technology*, Vol. 177, No. 3, 2005, pp. 485–511. doi:10.1080/00102200590909030

[7] Harrison, J., and Brewster, M. Q., "Infrared Emitted Intensity Measurements from Burning Aluminum Droplets in Solid Propellants," *Combustion Science and Technology*, Vol. 181, No. 1, 2009, pp. 18–35. doi:10.1080/00102200802415029

[8] Parry, D. L., and Brewster, M. Q., "Optical Constants of Al_2O_3 Smoke in Propellant Flames," *Journal of Thermophysics and Heat Transfer*, Vol. 5, No. 2, 1991, pp. 142–149. doi:10.2514/3.241

[9] Mills, A. F., *Heat Transfer*, 2nd ed., Prentice–Hall, Upper Saddle River, NJ, 1998.

[10] Qiu, T. Q., Longtin, J. P., and Tien, C. L., "Characteristics of Radiation Absorption in Metallic Particles," *Journal of Heat Transfer*, Vol. 117, No. 2, 1995, pp. 340–345. doi:10.1115/1.2822527

[11] Konopka, W. L., Reed, R. A., and Calia, V. S., "Measurements of Infrared Optical Properties of Al_2O_3 Rocket Particles," AIAA Paper 83-1568, 1983.

[12] Poletaev, N., and Florko, A., "Radiative Characteristics of an Aluminum Dust Flame. Condensed Phase," *Combustion, Explosion, and Shock Waves*, Vol. 43, No. 4, 2007, pp. 414–422.

doi:10.1007/s10573-007-0056-8
[13] Sarou-Kanian, V., Rifflet, J. C., and Millot, F., "IR Radiative Properties of Solid and Liquid Alumina: Effects of Temperature and Gaseous Environment," *International Journal of Thermophysics*, Vol. 26, No. 4, 2005, pp. 1263–1275. doi:10.1007/s10765-005-6725-5
[14] Bohren, C. F., and Huffman, D. R., *Absorption and Scattering of Light by Small Particles*, Wiley, New York, 1983.
[15] van de Hulst, H. C., *Light Scattering by Small Particles*, Dover, New York, 1981.
[16] Plass, G., "Temperature Dependence of the Mie Scattering and Absorption Cross Sections for Aluminum Oxide," *Applied Optics*, Vol. 4, No. 12, 1965, pp. 1616–1619. doi:10.1364/AO.4.001616
[17] Gryvnak, D., and Burch, D., "Optical and Infrared Properties of Al_2O_3 at Elevated Temperatures," *Journal of the Optical Society of America*, Vol. 55, No. 6, 1965, pp. 625–629. doi:10.1364/JOSA.55.000625
[18] Servaites, J., "Combustion of Aluminum Particles in Rocket Motor Oxidizers within a Shock Tube," Master's Thesis, Dept. of Mechanical and Industrial Engineering, Univ. of Illinois at Urbana–Champaign, Urbana, IL, 2001.
[19] Bazyn, T., Glumac, N., Krier, H., Ward, T., Schoenitz, M., and Dreizin, E., "Reflected Shock Ignition and Combustion of Aluminum and Nanocomposite Thermite Powders," *Combustion Science and Technology*, Vol. 179, No. 3, 2007, pp. 457–476. doi:10.1080/00102200600637261
[20] Parker, T., Foutter, R., and Rawlins, W., "A Pulsed Particle Injection System for Shock Tube Studies of Powders," *Review of Scientific Instruments*, Vol. 72, No. 1, 2001, pp. 263–267. doi:10.1063/1.1331327
[21] Brown, J., "Comparison of Ignition Characteristics of Pure and Coated Aluminum Powder in a Shock Tube Facility," M.S. Thesis, Dept. of Mechanical Science and Engineering, Univ. of Illinois at Urbana–Champaign, Urbana, IL, 2007.
[22] Bazyn, T., Krier, H., and Glumac, N., "Combustion of Nanoaluminum at Elevated Pressure and Temperature Behind Reflected Shock Waves," *Combustion and Flame*, Vol. 145, No. 4, 2006, pp. 703–713. doi:10.1016/j.combustflame.2005.12.017
[23] Jackson, T., Najjar, F., and Buckmaster, J., "New Aluminum Agglomeration Models and Their Use in Solid-Propellant-Rocket Simulations," *Journal of Propulsion and Power*, Vol. 21, No. 5, 2005, pp. 925–936. doi:10.2514/1.11888
[24] Strecker, J., and Roth, P., "Particle Breakup in Shock Waves Studied by Single Particle Light Scattering," *Particle and Particle Systems Characterization*, Vol. 11, No. 3, 1994, pp. 222–226. doi:10.1002/ppsc.19940110309
[25] Yan, Z., Wu, J., Hu, D., and Yang, X., "Agglomeration Evolution of Nano-Particles Aluminum in Normal Incident Shock Wave," *Chinese Physics Letters*, Vol. 23, No. 1, 2006, pp. 217–219. doi:10.1088/0256-307X/23/1/063
[26] Bakhir, L., Levashenko, G., and Tamanovich, V., "Effect of the Disperse Composition of Drops of Al_2O_3 in Flames on Their Coefficients of Absorption and Scattering," *Combustion, Explosion, and Shock Waves*, Vol. 12, No. 3, 1976, pp. 356–362. doi:10.1007/BF00789018
[27] Shigapov, A., "The Optical Properties of Aluminum Oxide at High Temperatures," *High Temperature*, Vol. 36, No. 1, 1998, pp. 35–39.
[28] Rosenberg, M., Smirnov, R., and Pigarov, A., "On Thermal Radiation from Heated Metallic Dust Grains," *Journal of Physics D: Applied Physics*, Vol. 41, No. 1, 2008, Paper 015202. doi:10.1088/0022-3727/41/1/015202
[29] Tanaka, Y., Smirnov, R., Pigarov, A., and Rosenberg, M., "Influence of Emissivity on Behavior of Metallic Dust Particles in Plasmas," *Physics of Plasmas*, Vol. 15, No. 7, 2008, Paper 073704–6. doi:10.1063/1.2946435
[30] Bauer, E., and Carlson, D., "Mie Scattering Calculations for Micron Size Alumina and Magnesia Spheres," *Journal of Quantitative Spectroscopy and Radiative Transfer*, Vol. 4, No. 3, 1964, pp. 363–374. doi:10.1016/0022-4073(64)90001-9
[31] Halpern, O., Lueneburg, R., and Clark, O., "On Multiple Scattering of Neutrons," *Physical Review*, Vol. 53, No. 2, 1938, pp. 173–183. doi:10.1103/PhysRev.53.173
[32] Gaseq: Software Package, Ver. 0.62, http://www.gaseq.co.uk [retrieved 4 Dec. 2009].
[33] Harrison, J., and Brewster, M. Q., "Simple Model of Thermal Emission from Burning Aluminum in Solid Propellants," *Journal of Thermophysics and Heat Transfer*, Vol. 23, No. 3, 2009, pp. 630–634. doi:10.2514/1.39143
[34] Whitson, M., "Handbook of the Infrared Optical Properties of Al_2O_3, Carbon, MgO, and ZrO_2," Vol. 1, Aerospace Corp., Rept. AD-A-013 722, El Segundo, CA, 1975.
[35] Grosshandler, W., and Monteiro, S., "Attenuation of Thermal Radiation by Pulverized Coal and Char," *Journal of Heat Transfer*, Vol. 104, No. 4, 1982, pp. 587–593. doi:10.1115/1.3245172
[36] Bazyn, T., Krier, H., and Glumac, N., "Evidence for the Transition from the Diffusion-Limit in Aluminum Combustion," *Proceedings of the Combustion Institute*, Vol. 31, No. 2, 2007, pp. 2021–2028. doi:10.1016/j.proci.2006.07.161
[37] Goroshin, S., Frost, D., and Levine, J., "Optical Pyrometry of Fireballs of Metalized Explosives," *Propellants, Explosives, Pyrotechnics*, Vol. 31, No. 3, 2006, pp. 169–181. doi:10.1002/prep.200600024